Record-level quantum efficiency from a high polarization strained GaAs/GaAsP superlattice photocathode with distributed Bragg reflector

Wei Liu, Yiqiao Chen, Wentao Lu, Aaron Moy, Matthew Poelker, Marcy Stutzman, and Shukui Zhang

Citation: Appl. Phys. Lett. **109**, 252104 (2016); doi: 10.1063/1.4972180
View online: http://dx.doi.org/10.1063/1.4972180
View Table of Contents: http://aip.scitation.org/toc/apl/109/25
Published by the American Institute of Physics

Record-level quantum efficiency from a high polarization strained GaAs/GaAsP superlattice photocathode with distributed Bragg reflector

Wei Liu,[1,2,3,a)] Yiqiao Chen,[4] Wentao Lu,[4] Aaron Moy,[4] Matthew Poelker,[3] Marcy Stutzman,[3] and Shukui Zhang[3]
[1]*Institute of Modern Physics, Chinese Academy of Sciences, 509 Nanchang Rd., Lanzhou 730000, China*
[2]*University of Chinese Academy of Sciences,19 A Yuquan Rd., Beijing 100049, China*
[3]*Thomas Jefferson National Accelerator facility, 12000 Jefferson Avenue, Newport News, Virginia 23606, USA*
[4]*SVT Associates, Inc., 7620 Executive Dr., Eden Prairie, Minnesota 55344, USA*

(Received 22 September 2016; accepted 30 November 2016; published online 20 December 2016)

Photocathodes that provide high electron-spin polarization (ESP) and high quantum efficiency (QE) can significantly enhance the physics capabilities of electron accelerators. We report record-level QE from a high-polarization strained GaAs/GaAsP superlattice photocathode fabricated with a Distributed Bragg Reflector (DBR). The DBR photocathode technique enhances the absorption of incident laser light thereby enhancing QE, but as literature suggests, it is very challenging to optimize all of the parameters associated with the fabrication of complicated photocathode structures composed of many distinct layers. Past reports of DBR photocathodes describe high polarization but typically QE of only ~1%, which is comparable to QE of high polarization photocathodes grown without a DBR structure. This work describes a strained GaAs/GaAsP superlattice DBR photocathode exhibiting a high polarization of 84% and significantly enhanced QE of 6.4%. *Published by AIP Publishing.* [http://dx.doi.org/10.1063/1.4972180]

Spin-polarized electron sources play a critical role in nuclear and high energy physics research, where the spin of the electron is used to study the nuclear structure, the dynamics of strong interactions, electro-weak nuclear physics, including parity-violation, and physics beyond the Standard Model.[1] Inexpensive bulk GaAs provides a very high quantum efficiency (QE), but the electron-spin polarization (ESP) cannot exceed 50% due to the heavy-hole, light-hole degeneracy of the $^2P_{3/2}$ valence band state.[2] Photocathodes grown on a crystal structure with a different lattice constant can provide beam polarization exceeding 50% because of the induced uniaxial strain that eliminates the degeneracy of the valence band.[3,4] Throughout the 1990s, single-strained-layer GaAs/GaAsP photocathodes providing polarization 75%–80% and maximum QE ~ 0.3%[3,5,6] were used at electron accelerators worldwide,[7–13] but the beam delivery using single-strained-layer photocathodes made apparent the delicate competing balance between maintaining the required degree of strain and growing of a layer thick enough to provide sufficient QE. In the following decade, strained superlattice structures consisting of very thin quantum-well active layers and alternating lattice-mismatched barrier layers were developed.[14] The superlattice structure maintained the required degree of strain to produce high polarization and also provided sufficient active layer thickness to obtain higher QE. The strained GaAs/GaAsP $_{0.36}$ superlattice structure reported in Ref. 15 provided QE of 1.2% with the polarization of 86%, and it is available commercially.[16] Strained superlattice photocathodes fabricated at other facilities have also demonstrated a very high polarization but no higher QE.[17–20]

One of the proposed Electron Ion Collider (EIC) designs, eRHIC,[21] requires milliamperes of polarized electron beam representing a factor of ~250 beyond today's state-of-the-art. A photocathode with a QE of only 1% would require ~8 W of laser light (with RF structure) to generate the desired 50 mA average beam current and even more light when photocathode QE decays during operation due to ion-bombardment.[22] In the standard strained superlattice design, most of the incident laser light simply heats the photocathode instead of promoting electron ejection, which can degrade QE due to the evaporation of the chemicals used to reduce the surface work function.[23] Methods to cool the photocathode during beam delivery are complicated because the photocathode is biased at high voltage. Developing photocathodes with enhanced QE could simplify the photogun design, reduce the drive-laser power requirements, and prolong the effective operating lifetime of the photogun.

A photocathode with a distributed Bragg reflector (DBR) was first proposed in 1993[24] and reported in the following years,[25,26] as a means to enhance the photocathode QE. The DBR serves to create a Fabry-Perot cavity formed by the front surface of photocathode and the DBR region. Instead of a single pass in the standard design, laser light of a particular wavelength reflects repeatedly within the Fabry-Perot cavity, which increases the beneficial absorption of the incident photons, and in principle, it leads to an enhanced QE. In our previous work,[27] the enhanced QE of strained GaAs/GaAsP superlattice photocathodes with DBRs was 1.2% with polarization near 90%. Relatively low QE was attributed to the weak resonant absorption of incident laser light and a mismatch between the wavelength of peak absorption and peak polarization. It was clear that the wavelength of peak reflectivity of the DBR was very sensitive to the refractive indices and thickness of each DBR layer constituent, and that the peak of resonant absorption was very sensitive to the thickness of the photocathode, especially the

a)Electronic mail: weiliu1006@yahoo.com

spacer layer between the DBR and the superlattice photocathode structures. Accurate control of the thickness of each layer and of the composition of each constituent chemical within the photocathode structure was challenging. In this study, a deeper appreciation for the global challenges of photocathode fabrication, together with improved modeling and fabrication techniques, allowed the fabrication of a strained GaAs/GaAsP superlattice photocathode with DBR (GaAsP/AlAsP) exhibiting significantly improved performance. The photocathode provided 84% polarization and QE of 6.4%, which is the highest QE of any reported high polarization photocathode. Moreover, peak polarization and QE were obtained at 776 nm, a wavelength compatible with CEBAF photogun drive lasers and readily available fiber-telecommunications hardware.

This DBR study benefited from the past work that resulted in the fabrication of the strained GaAs/GaAsP superlattice photocathode as described in Ref. 15, which represents the basis for polarization and QE comparison. See Ref. 15 for a complete description of the design criteria and optimization of this photocathode structure. A schematic layout of the strained GaAs/GaAsP superlattice photocathodes with and without DBR structure is shown in Figure 1.

The DBR is composed of multiple layers of alternating high and low indexes of refraction. A natural choice for high index of refraction layer was GaAsP, which provides a good lattice match to the graded buffer layer. Though a challenge for growth, we chose $AlAs_{1-y}P_y$ for the low index of refraction layer for a maximum refractive index contrast and a minimum DBR thickness. The thickness of each layer follows the quarter wavelength condition:[24] $n_H(\lambda_{DBR})d_H = \frac{\lambda_{DBR}}{4} = n_L(\lambda_{DBR})d_L$. The bandwidth for which the DBR exhibits high reflectivity is given by the formula

$$\Delta\lambda_{DBR} = \frac{4\lambda_{DBR}}{\pi}\sin^{-1}\left(\frac{n_H(\lambda_{DBR}) - n_L(\lambda_{DBR})}{n_H(\lambda_{DBR}) + n_L(\lambda_{DBR})}\right).$$

The Fabry-Perot cavity is formed by the vacuum/GaAs cap layer interface and the DBR. Proper thickness of a GaAsP spacer layer between GaAs/GaAsP superlattice and the DBR ensures the maximum absorption in the superlattice active layer that coincides with the central reflective wavelength of the DBR.

To design the structure, the refractive index of these layers can be estimated using the simplified interband transition model as a function of photon energy[28]

$$n(E)^2 = A\left[f(X_0) + \frac{1}{2}\left(\frac{E_0}{E_0+\Delta_0}\right)^{\frac{3}{2}} f(X_{so})\right] + B$$

with $f(X) = X^{-2}(2 - \sqrt{1+X} - \sqrt{1-X})$, $X_0 = \frac{E}{E_0}$, and $X_{so} = \frac{E}{E_0+\Delta_0}$, where, A represents the strength parameters of the $E/(E_0+\Delta_0)$ terms and B represents the nondispersive contribution arising from the higher-lying band gap $(E_1, E_1+\Delta_1, E_2,$ etc.) for each layer. The quantities E_0 and Δ_0 are the band-gap energy and spin-orbit splitting, respectively, given by the Vegard's Law for $GaAs_{1-x}P_x$.[29,30]

The desired wavelength of peak reflectivity was $\lambda_{DBR} \sim 780$ nm, compatible with the CEBAF drive lasers. Setting the phosphorus fractions in the $GaAs_{1-x}P_x$ and $AlAs_{1-y}P_y$ layers to 0.35 and 0.4, respectively, provided refractive indices of $n_H(780\,\text{nm}) = 3.4506$ and $n_L(780\,\text{nm}) = 2.9443$. From these parameters, the design values for the thickness of the $GaAsP_{0.35}$ and $AlAsP_{0.4}$ layers were 56.5 nm and 66.5 nm, respectively. Actual layer thicknesses were very close to these design values, 54 nm and 64 nm, which set the wavelength of peak reflectivity as λ_{DBR} of 755 nm, and the reflectivity bandwidth as $\Delta\lambda_{DBR} \sim 79$ nm. This implies the DBR can achieve a high reflectivity of >90% for wavelengths between 715 and 795 nm.

The transfer matrix method[31,32] was used to calculate the reflection, transmission, and absorption of the incident light through the complete multilayer thin-film structure including the GaAs substrate. Calculated values of surface reflectivity (R), transmittance (T) into the GaAs substrate, absorption (A) (not including the GaAs substrate), and the absorption enhancement factor as a function of wavelength are shown in Figure 2. There are two resonant absorption peaks within the optical cavity for the DBR photocathode at wavelengths 726 nm and 776 nm. Absorption by the substrate is not plotted as this process does not contribute to the polarized electron emission. The resonant peak at 776 nm is just 4 nm from the desired value of 780 nm. At 776 nm, the absorption is 21.03%, surface reflectivity is 50.14%, and transmittance into GaAs substrate is 28.83% for the DBR photocathode, corresponding to maximum electron spin polarization. The full-width half-maximum of the Fabry-Perot resonance is about 10 nm at 776 nm. The absorption enhancement factor is 7.4 at this wavelength.

To estimate the quantum efficiency of photocathode, one can solve the one-dimensional diffusion equations, based on the Spicer's three-step model[33,34]

GaAs	5 nm	p=5 × 10^{19} cm^{-3}
GaAs/GaAsP SL	(3.8/2.8 nm) ×14	p=5 × 10^{17} cm^{-3}
$GaAsP_{0.35}$	2750 nm	p=5 × 10^{18} cm^{-3}
Graded $GaAsP_x$ (x = 0~0.35)	5000 nm	p=5 × 10^{18} cm^{-3}
GaAs buffer	200 nm	p=2 × 10^{18} cm^{-3}
p-GaAs substrate (p>10^{18} cm^{-3})		

GaAs	5 nm	p=5 × 10^{19} cm^{-3}
GaAs/GaAsP SL	(3.8/2.8 nm) ×14	p=5 · 10^{17} cm^{-3}
$GaAsP_{0.35}$	750 nm	p=5 × 10^{18} cm^{-3}
$GaAsP_{0.35}$/ $AlAsP_{0.4}$ DBR	(54/64 nm) ×12	p=5 × 10^{18} cm^{-3}
$GaAsP_{0.35}$	2000 nm	p=5 × 10^{18} cm^{-3}
Graded $GaAsP_x$ (x = 0~0.35)	5000 nm	p=5 × 10^{18} cm^{-3}
GaAs buffer	200 nm	p=2 × 10^{18} cm^{-3}
p-GaAs substrate (p>10^{18} cm^{-3})		

FIG. 1. The schematic structure of the photocathodes: without DBR (left), with DBR (right).

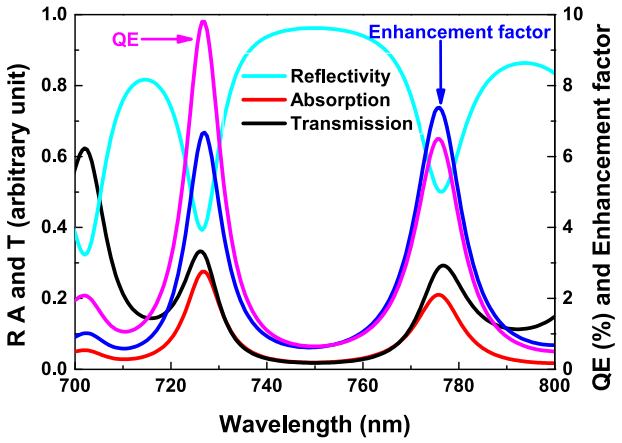

FIG. 2. Calculated values of absorption, reflectivity, and transmittance of the DBR photocathode, as a function of wavelength. Also shown, calculated QE and the enhancement factor compared to the photocathode without the DBR.

$$QE(\lambda) = \frac{P_L F_L A}{1+\frac{1}{\alpha_\lambda L_L}} + \frac{P_\Gamma \exp\left[k\left(-\frac{1}{1.42}-\frac{\lambda}{1240}\right)\right]A}{1+\frac{1}{\alpha_\lambda L_\Gamma}} \times \left[F_\Gamma + \frac{F_L L_\Gamma}{\alpha_\lambda F_L (L_\Gamma + L_L)\left(1+\frac{1}{\alpha_\lambda L_L}\right)}\right],$$

where P_Γ and P_L are the surface electron escape probability for the Γ and L minima, respectively, which are independent of the incident photon energy, F_Γ is the remaining fraction of excited electrons, F_L is the fraction of electrons that is excited to energies greater than the L minima, A is the absorption of photocathode, L_Γ and L_L are the electron diffusion length for the Γ and L minima, respectively, α_λ is the absorption coefficient of the photocathode, and k is a coefficient ($k \geq 0$). The calculated QE for the DBR photocathode, together with the QE enhancement factor as a function of wavelength, is shown in Figure 2.

All photocathodes were grown in a solid-source molecular beam epitaxy (SSMBE) system equipped with As and P crackers on a (100) p-type GaAs substrate, upon which a 200 nm Be-doped (2×10^{18} cm^{-3}) GaAs buffer layer was deposited. The 5-μm-thick Be-doped graded $GaAsP_x$ layer was then grown with an increasing P composition from $x = 0$ to 0.35, followed by a 2-μm-thick $GaAs_{0.65}P_{0.35}$ layer, in order to produce a strain-relaxed $GaAs_{0.65}P_{0.35}$ layer compatible with the superlattice active layer. The DBR structure consisting of 12 pairs of $GaAs_{0.65}P_{0.35}$ (54 nm)/$AlAs_{0.6}P_{0.4}$ (64 nm) was subsequently grown on top of this layer. In order to create an effective Fabry-Perot resonant cavity for the desired wavelength near 780 nm, a 750-nm-thick $GaAs_{0.65}P_{0.35}$ layer was grown on top of DBR, acting as a spacer. Both $GaAs_{0.65}P_{0.35}$ and DBR layers were Be-doped at 5×10^{18} cm^{-3} to promote high electrical conductivity. The p-type (5×10^{17} cm^{-3}) GaAs (3.8 nm)/$GaAs_{0.65}P_{0.35}$ (2.8 nm) superlattice layer was positioned between the $GaAs_{0.65}P_{0.35}$ spacer and the 5-nm-thick GaAs cap layer doped at $p = 5 \times 10^{19}$ cm^{-3}. The only difference between the DBR photocathode and the non-DBR photocathode was the 12 pairs of $GaAs_{0.65}P_{0.35}$ (54 nm)/$AlAs_{0.6}P_{0.4}$ (64 nm) layers.

The growth of $GaAs_{0.65}P_{0.35}$/$AlAs_{0.6}P_{0.4}$ DBR structure was very challenging due to the large differences in growth temperatures and the V/III flux ratios for the $GaAs_{0.65}P_{0.35}$ and $AlAs_{0.6}P_{0.4}$ layers. The optimal growth temperatures for $GaAs_{0.65}P_{0.35}$ and $AlAs_{0.6}P_{0.4}$ were 660–700 °C and 700–750 °C, respectively, as determined by the surface temperature measurement and reflective high energy electron diffraction (RHEED) images during the MBE growth. Thicknesses and composition were verified using x-ray diffraction measurements and x-ray simulation models. It was very difficult to accurately control the growth rate of $GaAs_{0.65}P_{0.35}$ at high temperatures, especially approaching at 700 °C, because the re-evaporation rate of Ga atoms from the sample surface increases rapidly with increasing growth temperatures above 660 °C resulting in inconsistent control of the layer thickness. Additionally, maintaining the As/P fraction in $GaAs_{0.65}P_{0.35}$ layers is difficult when grown below 650 °C, as the As/P fraction is very sensitive at low growth temperatures.[35,36] For this reason, the thick graded composition GaAsP was grown at 660 °C. However, the material quality of $AlAs_{0.6}P_{0.4}$ layer was poor when grown at this temperature. Therefore, the growth temperature of $GaAs_{0.65}P_{0.35}$/$AlAs_{0.6}P_{0.4}$DBR had to be kept at 700 °C as measured by an SVT AccuTemp process monitor using a two-color infrared pyrometer. The large difference in V/III flux ratio during the growth between $GaAs_{0.65}P_{0.35}$ and $AlAs_{0.6}P_{0.4}$ added extra difficulty to achieving high quality DBR layers. The V/III ratio for $GaAs_{0.65}P_{0.35}$ is around 50, whereas the ratio is only around 3 for $AlAs_{0.6}P_{0.4}$. Numerous growth-calibration and material-characterization runs were required to develop a suitable substrate temperature and source-switching recipes to enable the fabrication of high quality $GaAs_{0.65}P_{0.35}$/$AlAs_{0.6}P_{0.4}$ DBR and strained superlattice structures grown by SSMBE.

Photocathode samples were evaluated using a low-voltage retarding-field Mott polarimeter.[37] Samples were attached to sample holders and installed within the vacuum chamber, which was baked at 250 °C for 36 h, and allowed to cool to room temperature. Photocathodes were then heated to 480 °C to remove the As cap and cooled to room temperature under typical vacuum pressure $\sim 10^{-11}$ Torr. A negative electron affinity condition was obtained using the standard yo-yo activation procedure with cesium and NF_3.[38] A broadly tunable super-continuum laser (NKT Photonics, SuperK) provided the milli-Watts of output power over the wavelength range from 400 to 800 nm. Optical waveplates (quarter and halfwave) were used to generate the left and right circularly polarized light required to obtain spin polarized electrons.

Measured values of QE and electron-spin polarization (ESP) as a function of wavelength, for photocathodes with and without DBR, are shown in Figure 3(a). For the non-DBR photocathode, results are consistent with past work[15] indicating the peak polarization of 90% and the QE of 0.89% at a wavelength of ~780 nm. In stark contrast, the QE of the DBR photocathode shows the telltale prominent oscillatory behavior indicative of resonant absorption. Measured reflectivity and QE enhancement (i.e., the ratio of QE values of photocathodes with and without DBR) are shown in Figure 3(b). The two dips in the reflectivity spectrum are clearly correlated

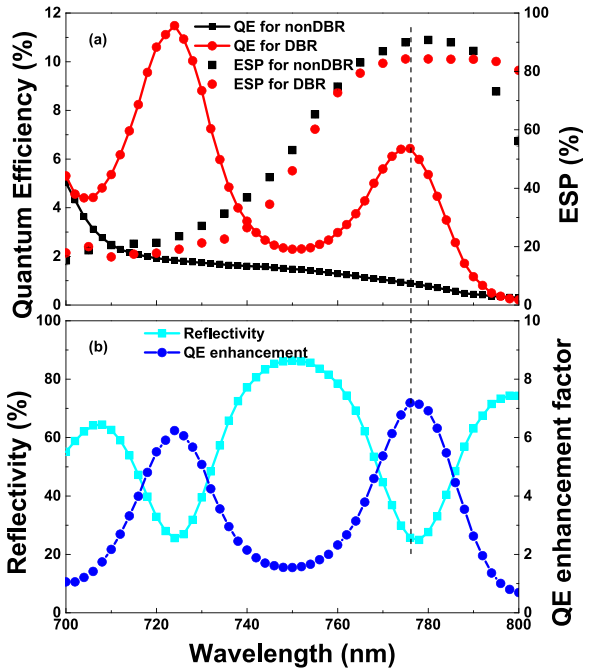

FIG. 3. (a) The QE and electron-spin polarization (ESP) for the strained GaAs/GaAsP superlattice photocathodes with and without DBR as a function of the wavelength; (b) Reflectivity and QE enhancement factor of DBR photocathode as a function of the wavelength. The dash line indicates the resonant position.

TABLE I. Figure of merit for polarized electron sources.

Cathode	Reference	P (%)	QE (%)	P^2QE (%)
GaAs-GaAs$P_{0.36}$	SLAC/SVT[15]	86	1.2	0.89
GaAs-GaAs$P_{0.38}$	Nagoya[20]	92	1.6	1.35
$Al_{0.19}In_{0.2}$GaAs-$Al_{0.4}$GaAs	St. Peterburg[18]	92	0.85	0.72
GaAs-ga$AsP_{0.35}$ (with DBR)	JLab/SVT	84	6.4	4.52

with wavelength locations of QE maxima. At the wavelength of interest, 776 nm, the QE was 6.4% and the polarization was ~84%. The measured QE enhancement of ~7.2 is very close to the predicted value of ~7.4. It should be noted that QE enhancement is a somewhat arbitrary metric dependent on when measurements were made following photocathode activation and subject to non-trivial variations in QE associated with vacuum conditions that influence the photocathode lifetime.

These results are compared to results from other photocathodes listed in Table I, showing QE, polarization, and photocathode Figure of Merit (P^2QE). The Figure of Merit of our photocathode is a factor of four higher than the last highest value. In conclusion, a QE of 6.4% is the highest reported value of any high polarization photocathode. Precise control of the thickness of each layer and the composition of each constituent led to these improved results. Further optimization should lead to even higher QE, and polarization values approaching the best values from superlattice photocathodes without DBR structures.

Authored by Jefferson Science Associates, LLC under U.S. DOE Contract No. DE-AC05-06OR23177. The U.S. Government retains a non-exclusive, paid-up, irrevocable, world-wide license to publish or reproduce this manuscript for U.S. Government purposes. SVT Associates was funded by the U.S. DOEs Office of Nuclear Physics SBIR program DE-SC0009516. W. Liu is currently conducting research at Jefferson Lab toward a Ph.D. degree.

[1]H. Montgomery, J. Phys.: Conf. Ser. **299**, 011001 (2011).
[2]D. T. Pierce and F. Meier, Phys. Rev. B **13**, 5484 (1976).
[3]T. Nakanishi, H. Aoyagi, H. Horinaka, Y. Kamiya, T. Kato, S. Nakamura, T. Saka, and M. Tsubata, Phys. Lett. A **158**, 345 (1991).
[4]T. Maruyama, E. L. Garwin, R. Prepost, G. H. Zapalac, J. S. Smith, and J. D. Walker, Phys. Rev. Lett. **66**, 2376 (1991).
[5]See http://www.bandwidthsemi.com for Bandwidth Semiconductor.
[6]T. Maruyama, E. L. Garwin, R. Prepost, and G. H. Zapalac, Phys. Rev. B **46**, 4261 (1992).
[7]K. Aulenbacher, Ch. Nachtigall, H. G. Andresen, J. Bermuth, Th. Dombo, P. Drescher, H. Euteneuer, H. Fischer, D. V. Harrach, P. Hartmann, *et al.*, Nucl. Instrum. Methods, A **391**, 498 (1997).
[8]G. D. Cates, V. W. Hughes, R. Michaels, H. R. Schaefer, T. J. Gay, M. S. Lubell, R. Wilson, G. W. Dodson, K. A. Dow, S. B. Kowalski, *et al.*, Nucl. Instrum. Methods, A **278**, 293 (1989).
[9]E. Tsentalovich, D. Barkhuff, J. Chen, G. Dodson, M. Farkhondeh, W. Franklin, E. Ihloff, F. Kaertner, C. Tschalaer, B. Yang, and T. Zwart, Nucl. Instrum. Methods, A **582**, 413 (2007).
[10]M. J. J. van den Putte, C. W. De Jager, S. G. Konstantinov, V. Ya. Korchagin, F. B. Kroes, E. P. vanLeeuwen, B. L. Militsyn, N. H. Papadakis, S. G. Popov, G. V. Serdobintsev *et al.*, AIP Conf. Proc. **421**, 260 (1998).
[11]W. Hillert, M. Govin, and B. Neff, AIP Conf. Proc. **570**, 961 (2001).
[12]C. K. Sinclair, P. A. Adderley, B. M. Dunham, J. C. Hansknecht, P. Hartmann, M. Poelker, J. S. Price, P. M. Rutt, W. J. Schneider, and M. Steigerwald, Phys. Rev. ST Accel. Beams **10**, 023501 (2007).
[13]R. Alley, H. Aoyagi, J. Clendenin, J. Frisch, C. Garden, E. Hoyt, R. Kirby, L. Klaisner, A. Kulikov, R. Miller *et al.*, Nucl. Instrum. Methods, A **365**, 1 (1995).
[14]T. Omori, Y. Kurihara, Y. Takeuchi, M. Yoshioka, t. Nakanishi, S. Okumi, M. tsubata, M. Tawada, K. Togawa, Y. Tanimoto, C. Takahashi, T. Baba, and M. Mizuta, Jpn. J. Appl. Phys. **33**, 5676 (1994).
[15]T. Maruyama, D. A. Luh, A. Brachmann, J. E. Clendenin, E. L. Garwin, S. Harvey, J. Jiang, R. E. Kirby, C. Y. Prescott, R. Prepost, and A. M. Moy, Appl. Phys. Lett. **85**, 2640 (2004).
[16]See http://www.svta.com/ for SVT Associated, Inc.
[17]A. V. Subashiev, L. G. Gerchikov, Y. A. Mamaev, Y. P. Yashin, J. S. Roberts, D.-A. Luh, T. Maruyama, and J. E. Clendenin, Appl. Phys. Lett. **86**, 171911 (2005).
[18]Yu. A. Mamaev, L. G. Gerchikov, Yu. P. Yashin, D. A. Vasiliev, V. V. Kuzmichev, V. M. Ustinov, A. E. Zhukov, V. S. Mikhrin, and A. P. Vasiliev, Appl. Phys. Lett. **93**, 081114 (2008).
[19]X. G. Jin, A. Mano, F. Ichihashi, N. Yamamoto, and Y. Takeda, Appl. Phys. Express **6**, 015801 (2013).
[20]X. G. Jin, B. Ozdol, M. Yamamoto, A. Mano, N. Yamamoto, and Y. Takeda, Appl. Phys. Lett. **105**, 203509 (2014).
[21]E. C. Aschenauer, M. D. Baker, A. Bazilevsky, K. Boyle, S. Belomestnykh, I. Ben-Zvi, S. Brooks, C. Brutus, T. Burton, S. Fazio *et al.*, e-print arXiv:1409.1633.
[22]W. Liu, S. Zhang, M. L. Stutzman, and M. Poelker, "The effects of ion bombardment on bulk GaAs photocathodes with different surface-cleavage planes," Phys. Rev. Accel. Beams **19**, 103402 (2016).
[23]S. Zhang, S. V. Benson, and C. H-Garcia, Nucl. Instrum. Methods, A **631**, 22 (2011).
[24]T. Saka, T. Kato, T. Nakanishi, M. Tsubata, K. Kishino, H. Horinaka, Y. Kamiya, S. Okumi, C. Takahashi, Y. Tanimoto *et al.*, Jpn. J. Appl. Phys. **32**, 1837 (1993).
[25]J. C. Grobli, D. Oberli, and F. Meier, Phys. Rev. Lett. **74**, 2106 (1995).
[26]L. G. Gerchikov, K. Aulenbacher, J. E. Clendenin, V. V. Kuzmichev, Y. A. Mamaev, T. Maruyama, V. S. Mikhrin, J. S. Roberts, V. M. Ustinov, D. A. Vasilev, A. P. Vasiliev, Y. P. Yashin, and A. E. Zhukov, AIP Conf. Proc. **980**, 124 (2008).
[27]S. Zhang, M. L. Stutzman, M. Poelker, Y. Chen, and A. Moy, in Proceedings of the IPAC2015, Richmond, USA (2015).
[28]S. Adachi, *Properties of Semiconductor Alloys: Group-IV, III-V and II-VI Semiconductors* (Wiley, 2009), p. 238.
[29]M. Levinshtein, S. Rumyantsev, and M. Shur, *Handbook Series on Semiconductor Parameters* (World Scientific, 1996).
[30]I. Vurgaftman, J. R. Meyer, and L. R. Ram-Mohan, J. Appl. Phys. **89**, 5815 (2001).

[31]H. A. Macleod, *Thin-Film Optical Filters*, 4th ed. (CRC Press, 2010).
[32]P. Peumans, A. Yakimov, and S. R. Forrest, J. Appl. Phys. **93**, 3693 (2003).
[33]J. Zou, B. Chang, H. Chen, and L. Liu, J. Appl. Phys. **101**, 033126 (2007).
[34]J. Zou, B. Chang, Z. Yang, Y. Zhang, and J. Qiao, J. Appl. Phys. **105**, 013714 (2009).
[35]B. W. Liang and C. W. Tu, J. Appl. Phys. **74**, 255 (1993).
[36]S. Tomasulo, J. Simon, P. J. Simmonds, J. Biagiotti, and M. L. Lee, J. Vac. Sci. Technol. B **29**, 03C118 (2011).
[37]J. L. McCarter, M. L. Stutzman, K. W. Trantham, T. G. Anderson, A. M. Cook, and T. J. Gay, Nucl. Instrum. Methods, A **618**, 30 (2010).
[38]R. L. Bell, *Negative Electron Affinity Devices* (Clarendon, Oxford, England, 1973).